

Radio Spectra of Three Supernova Remnants: G114.3+0.3, G116.5+1.1 and G116.9+0.2

Wen-Wu Tian^{1,2} and Denis Leahy²

¹ National Astronomical Observatories, Chinese Academy of Sciences, Beijing 100012; tww@bao.ac.cn

² Department of Physics & Astronomy, University of Calgary, Calgary, Alberta T2N 1N4, Canada

Abstract Presented are new images of supernova remnants G114.3+0.3, G116.5+1.1 and G116.9+0.2 (CTB 1) at 408 MHz from the Canadian Galactic Plane Survey (CGPS). We also use the 1420 MHz images from the CGPS in a study of their 408–1420 MHz spectral indices. The flux densities at 408 MHz and 1420 MHz, corrected for flux densities from compact sources within the SNRs, are 12 ± 6 Jy and 9.8 ± 0.8 Jy for G114.3+0.3, 15.0 ± 1.5 Jy and 10.6 ± 0.6 Jy for G116.5+1.1, 15.0 ± 1.5 Jy and 8.1 ± 0.4 Jy for G116.9+0.2. The integrated flux density-based spectral indices ($S_\nu \propto \nu^{-\alpha}$) are $\alpha = 0.16 \pm 0.41$, 0.28 ± 0.09 and 0.49 ± 0.09 for G114.3+0.3, G116.5+1.1 and G116.9+0.2, respectively. Their T - T plot-based spectral indices are 0.68 ± 0.48 , 0.28 ± 0.15 , and 0.48 ± 0.04 , in agreement with the integrated flux density-based spectral indices. New flux densities are derived at 2695 MHz which are significantly larger than previous values. The new 408, 1420 and 2695 MHz flux densities and published values at other frequencies, where images are not available, are fitted after correcting for contributions from compact sources, to derive their multi-frequency spectral indices.

Key words: ISM: individual G114.3+0.3, G116.5+1.1, G116.9+0.2 — radio continuum: ISM

1 INTRODUCTION

As one of the systematic efforts to study the spectral index variation of supernova remnants (SNRs), we report new CGPS (Canadian Galactic Plane Survey) radio observations of three shell-type SNRs, namely, G114.3+0.3, G116.5+1.1 and G116.9+0.2 (CTB 1). They are located within a field of $4^\circ \times 2.5^\circ$, and their radio spectra have not been studied in detail before. G116.9+0.2 (CTB 1) has been extensively studied in both radio (e.g. Yar-Uyaniker et al. 2004) and optical emission (e.g. Fesen et al. 1997). G114.3+0.3 and G116.5+1.1, due to their low surface brightness and large diameter, are less well studied (Reich & Braunsfurth 1981; Yar-Uyaniker et al. 2004; Mavromatakis et al. 2005). Reich & Braunsfurth (1981) gave their images and physical properties at 1420 MHz with HPBW 9×9 arcmin and 2696 MHz with 4.6×4.6 arcmin using the Effelsberg 100-m telescope. Yar-Uyaniker et al. (2004) presented their continuum and HI images at 1420 MHz with HPBW about 1 arcmin from the CGPS, mainly emphasizing distance estimates. Mavromatakis et al. (2005) presented optical and HI observations of G116.5+1.1.

In this paper, we use both the 408 MHz and 1420 MHz data from the CGPS, and the 2695 MHz data from the Effelsberg 100-m telescope (Fürst et al. 1990) in a study of the radio spectra of the three SNRs.

2 OBSERVATIONS AND IMAGE ANALYSIS

The 408 MHz and 1420 MHz data sets come from the CGPS, which was described in detail by Taylor et al. (2003). The data sets are mainly based on observations from the Synthesis Telescope (ST) of the Dominion Radio Astrophysical Observatory (DRAO). The spatial resolution is better than $1' \times 1'$ cosec(δ) at 1420 MHz and $3.4' \times 3.4'$ cosec(δ) at 408 MHz. DRAO ST observations are not sensitive to structures larger than an angular size scale of about 3.3° at 408 MHz and $56'$ at 1420 MHz. Thus the CGPS includes data from the 408 MHz all-sky survey of Haslam et al (1982) which has an effective resolution of $51'$ and

the Effelsberg 1.4 GHz Galactic plane survey of Reich et al. (1990, 1997) with resolution $9.4'$ for large scale emission (the single-dish data are freely available at <http://www.mpifr-bonn.mpg.de/survey.html>).

We analyze the images and determine flux densities using the DRAO export software package. Two of our previous papers (Tian & Leahy 2005; Leahy & Tian 2005) have given a detailed description of the methods to reduce the influence of compact sources within the SNRs on the radio spectrum.

3 RESULTS

3.1 Structure at 408 MHz and 1420 MHz

The CGPS images at 408 MHz and 1420 MHz are shown in Figure 1. The left panels show the 408 MHz maps, the right panels show the 1420 MHz maps. For reference we also reproduce the 2695 MHz Effelsberg map of the three SNRs in Figure 2 (from the Effelsberg public database, Fürst et al. 1990). The Effelsberg map has a resolution of $4.3'$. The 408 MHz images are seen here for the first time. G114.3+0.3 (Fig. 1, top panels) is only faintly visible at 408 MHz, but 408 MHz emission is clearly seen from S165 and the bright 1420 MHz southeast limb. Comparing with the 1420 MHz image, faint 408 MHz emission from G114.3+0.3 is seen along the northwest limb and the southeast interior. The strong 408 MHz background, especially in the southern half of the image, makes G114.3+0.4 difficult to see except by comparison with the 1420 MHz structure. There is a bright emission region at $l = 113.6$, $b = -0.7$, which is the HII region S163 (Lockman 1989).

G116.5+1.1 (Fig. 1, middle panels) is more clearly visible at 408 MHz. It shows essentially the same features as at 1420 MHz with bright north to northeast limb, bright southern interior, and faint west to southwest limb. For both G114.3+0.3 and G116.5+1.1 bright compact sources contribute significantly to the flux density (see especially the 1420 MHz map for the number of compact sources across the face of these SNRs). At lower spatial resolution the compact sources would be confused with the diffuse spatial emission of these SNRs.

G116.9+0.2 (CTB 1, Fig. 1, lower panels) is a bright SNR and has clearly defined shell structure at 408 MHz which is fully consistent with the 1420 MHz structure convolved to the lower resolution of the 408 MHz data. Compact sources contribute to the flux density mainly along the southern limb and the southern interior filament.

3.2 T - T Plot Spectral Indices

Bright compact sources affect both integrated flux density for the SNRs and spectral indices, so we correct for the effects of compact sources below. First we consider the spectral index between 408 MHz and 1420 MHz based on the T - T plot (for a description of the T - T plot method see e.g. Leahy & Roger 1998). For the T - T plot analysis, first a single region for the whole of the SNR is used, as shown in Figure 1. The T - T plots for the three SNRs are shown in Figure 3 (G114.3+0.3 left; G116.5+1.1 middle; G116.9+0.2 right). Two cases are considered: using all pixels including the compact sources; and excluding the compact sources. The compact sources' influence on the T - T plots is clearly seen in Figure 1. When we quote spectral index errors, we combine the formal error from the fit to the T - T plot with the spectral index error of $\simeq 0.03$ arising from the calibration errors of the 408 and 1420 MHz flux densities. In most cases, the former error dominates.

Next, the SNRs are subdivided into smaller areas as labelled in Figure 1 to search for spatial variations in the spectral index. Table 1 lists the results for both cases of analysis: including and excluding the compact sources. The results in the two cases are not very different. By inspecting the T - T plots shown in Figure 3, this near agreement can be seen to be just due the mixing of steep and flat spectral indices in the compact sources. In our other studies of spectral indices of SNRs (Tian & Leahy 2005; Leahy & Tian 2005; Tian & Leahy 2006), the compact sources generally had significantly steeper spectral indices than the SNRs, so the correct analysis did produce different spectral indices. From now on we discuss spectral indices derived with the compact sources removed, unless specified otherwise. We also carry out a T - T plot analysis for S163 and we verify it has a thermal spectral index similar to S165.

3.3 Integrated Flux Densities and Spectral Indices

From the 408 MHz and 1420 MHz maps we have derived integrated flux densities for the three SNRs with diffuse background subtracted. The resulting 408 MHz to 1420 MHz spectral indices, using flux densi-

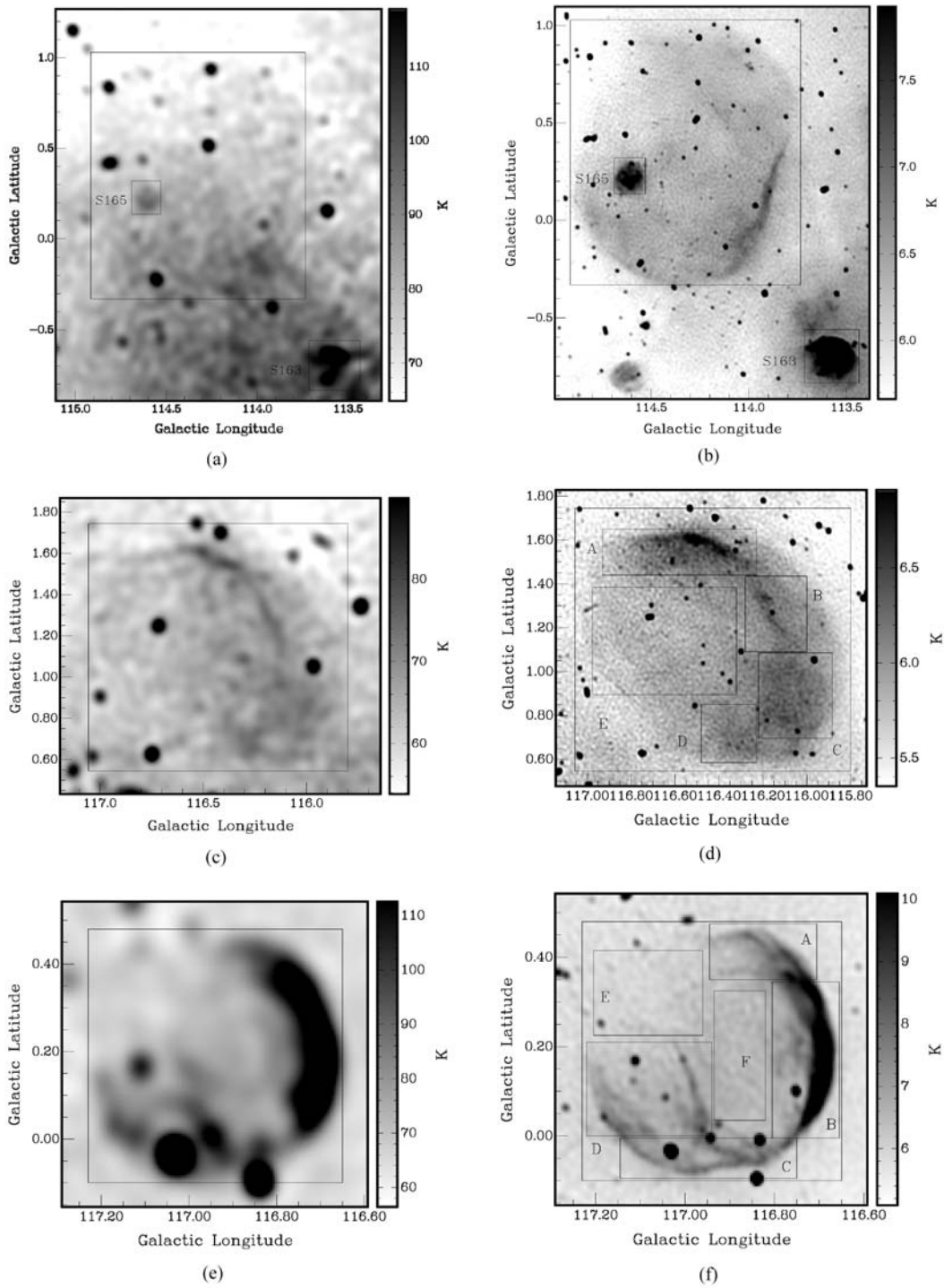


Fig. 1 First row shows G114.3+0.3 at 408 MHz (left) and 1420 MHz (right), second row for G116.5+1.1 and the third for G116.9+0.2. The large boxes used for whole SNR T - T plots are shown in the 408 MHz images. The smaller boxes, labelled with letters and used for sub-area T - T plots, are shown in the 1420 MHz images.

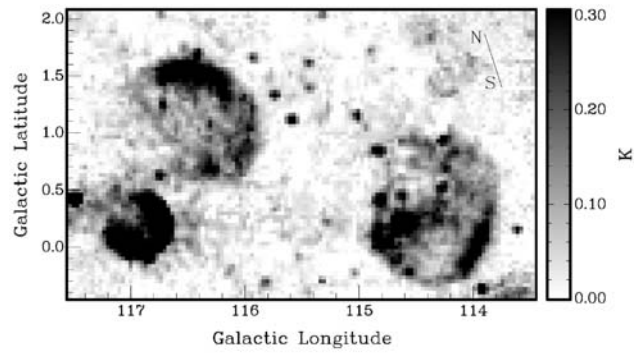


Fig. 2 The 2695 MHz Effelsberg map of the three supernova remnants, G114.3+0.3, G116.5+1.1 and G116.9+0.2 (CTB 1). The N-S direction is marked on the upper right.

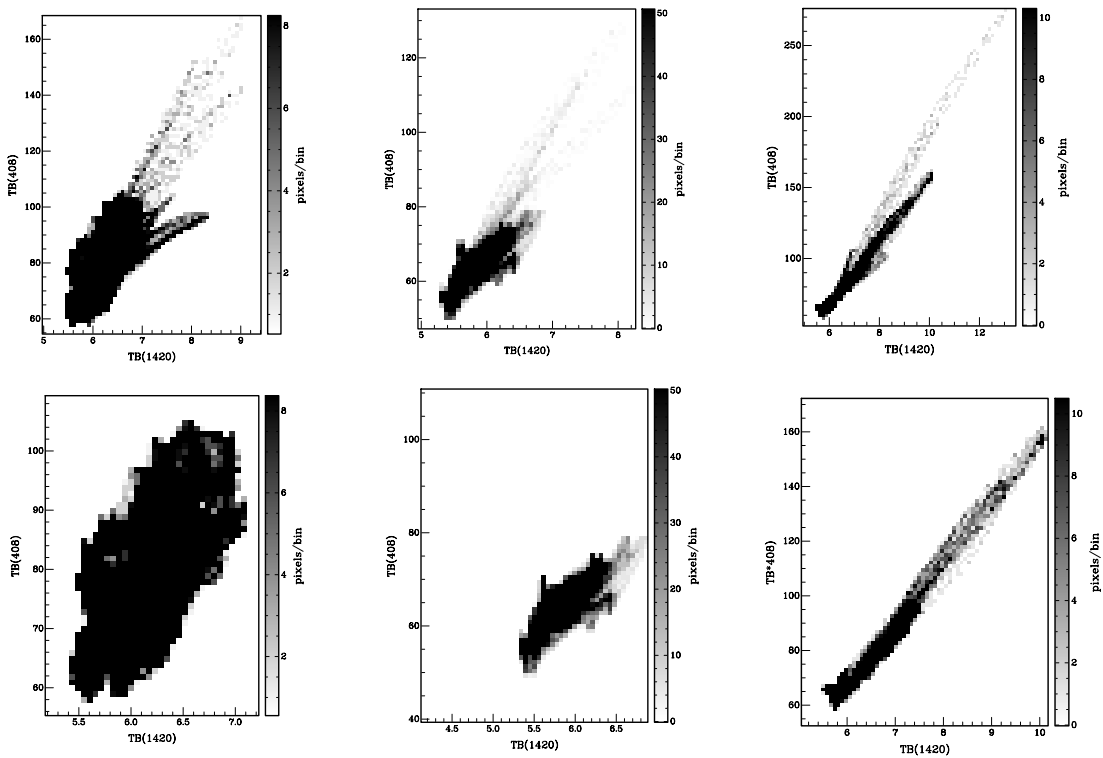


Fig. 3 Whole SNR 408–1420 MHz T - T plots for three SNRs. Plots in the top (bottom) row are for maps including (excluding) compact sources. The values of α including and excluding the compact sources are $(0.64 \pm 0.34, 0.68 \pm 0.48)$ for G114.3+0.3 (left), $(0.34 \pm 0.15, 0.28 \pm 0.15)$ for G116.5+1.1 (center), and $(0.51 \pm 0.04, 0.48 \pm 0.04)$ for G116.9+0.2 (right).

ties without compact sources, are 0.16 ± 0.41 for G114.3+0.3, 0.28 ± 0.09 for G116.5+1.1, and 0.49 ± 0.09 for G116.9+0.2. Table 2 lists the flux densities and spectral indices for the SNRs and the compact sources within each SNR.

Table 1 408–1420 MHz T - T Plot Spectral Indices with and without Compact Sources (CS)

Area	α	
	including CS	CS removed
All G114.3+0.3	$0.64 \pm 0.34^*$	0.68 ± 0.48
For G116.5+1.1		
A	0.26 ± 0.19	0.26 ± 0.19
B	0.41 ± 0.20	0.40 ± 0.27
C	0.23 ± 0.35	0.16 ± 0.32
D	0.56 ± 0.23	0.56 ± 0.23
E	0.55 ± 0.20	0.48 ± 0.21
All G116.5+1.1	0.34 ± 0.15	0.28 ± 0.15
For G116.9+0.2		
A	0.55 ± 0.04	0.55 ± 0.04
B	0.50 ± 0.04	0.50 ± 0.04
C	0.76 ± 0.04	0.38 ± 0.04
D	0.57 ± 0.08	0.45 ± 0.04
E	0.11 ± 0.31	0.11 ± 0.31
F	0.63 ± 0.05	0.75 ± 0.14
All G116.9+0.4	0.51 ± 0.04	0.48 ± 0.04

*includes S165.

Table 2 Integrated Flux Densities and Spectral Indices of G114.3+0.3 (G114), G116.5+1.1 (G116.5), G116.9+0.2 (CTB 1), and Compact Sources (CS) within Three SNRs

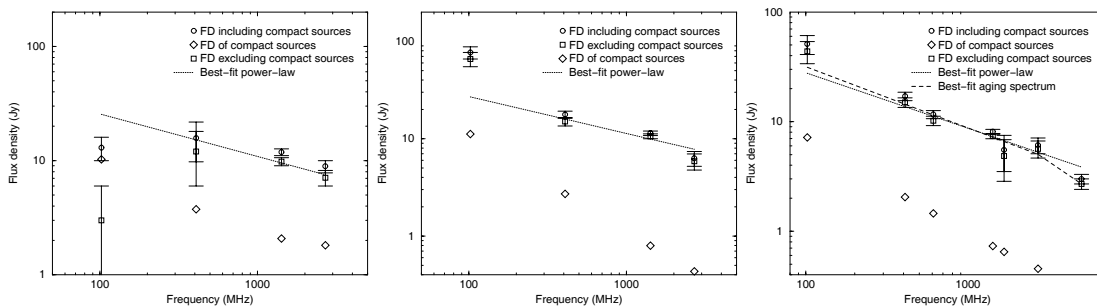
Freq.	G114	G114's CS*	G114+CS*	G116.5	G116.5's CS	G116.5+CS	CTB 1	CTB 1's CS	CTB 1+CS
MHz	Jy								
408	12.0 ± 6.0	3.75 ± 0.24	15.8 ± 6.2	15.0 ± 1.5	2.71 ± 0.15	17.7 ± 1.7	15.0 ± 1.5	2.05 ± 0.13	17.1 ± 1.6
1420	9.8 ± 0.8	2.08 ± 0.09	11.5 ± 0.9	10.6 ± 0.6	0.79 ± 0.03	11.4 ± 0.6	8.1 ± 0.4	0.73 ± 0.05	8.8 ± 0.5
α	0.16 ± 0.41	0.47 ± 0.06	0.25 ± 0.32	0.28 ± 0.09	0.99 ± 0.05	0.35 ± 0.09	0.49 ± 0.09	0.83 ± 0.07	0.50 ± 0.07

* includes S165

4 DISCUSSION

4.1 G114.3+0.3

Published integrated flux densities for G114.3+0.3 at other frequencies are given in Table 3. Figure 4 (left) shows the flux densities before and after correcting for the flux density of the compact sources. We carry out

**Fig. 4** Radio spectra of G114.3+0.3 (left), G116.5+1.1 (middle) and G116.9+0.2 (right). G114.3+0.3 has a best-fit spectral index $\alpha=0.37$, G116.5+1.1, $\alpha=0.38$ and G116.9+0.2, $\alpha=0.51$ (see text for details).

all spectral fits here for all three SNRs using fluxes with compact sources removed. The best fit power-law spectrum to all four flux-densities gives a spectral index of -0.1 and $\chi^2=8$. The 102 MHz point is well below the power law fit. Referring to Figure 1, one can see a strong steep spectrum background in the southern half of the G114.3+0.3 408 MHz image. Also at the higher spatial resolution of the 1420 MHz map, there is a faint background just outside the south and west limb, but it rises to high values further out. If one viewed G114.3+0.3 at low spatial resolution, such as in the 102 MHz observation, one would see the bright emission south and west of G114.3+0.3 smeared into the faint background just outside the limb. This would cause one to overestimate the background. Thus the flux density at 102 MHz should be higher than the published value. A spectral fit to the data without the 102 MHz point gives a spectral index of 0.37 (90% uncertainty range 0.05 to 0.66). This spectral fit is shown in Figure 4 (left). This value is consistent with the 408–1420 MHz spectral index from the T - T plot of 0.7 ± 0.5 and from 408 and 1420 MHz integrated fluxes (0.16 ± 0.41). The various spectral index measurements all have large uncertainties, due to the faintness of G114.3+0.3 and the high background in the region.

Table 3 Integrated Flux Densities (FD) of G114.3 + 0.3

Freq. MHz	Beamwidth arcmin	FD Jy	References
102.0	48×25	13.0±3.0	1994, Kovalenko et al.
408.0	3.4×3.9	12.0±6.0*	this paper
1420.0	9×9	5.3±0.8	1981, Reich & Braunfurth
1420.0	1×1.13	9.8±0.8*	this paper
2695	4.3×4.3	8.9±1.2	see text
2700.0	4.6×4.6	4.4±0.4	1981, Reich & Braunfurth

4.2 G116.5+1.1

The integrated flux densities of G116.5+1.1 are given in Table 4. The best fit α to all four data points is 0.48 with $\chi^2=15$. The 102 MHz point is well above the best fit power-law. The spectral fit to the data, omitting the 102 MHz point, gives $\alpha=0.38$ ($\chi^2=4.7$) and 90% uncertainty range 0.25 to 0.50. This value is consistent with the 408–1420 MHz spectral index from the T - T plot of 0.28 ± 0.15 and from 408 and 1420 MHz integrated fluxes of 0.28 ± 0.09 . Figure 4 (middle) shows the radio spectrum corrected for compact sources and the best fit power law spectrum ($\alpha=0.38$). Table 1 lists the T - T plot spectral indices for the subregions of G116.5+1.1. They are all consistent within the errors with the whole SNR T - T plot value of 0.28 ± 0.15 . So there is no evidence for spectral index variations in G116.5+1.1 to the level of $\simeq 0.2$ in spectral index.

Table 4 Integrated Flux Densities (FD) of G116.5+1.1

Freq. MHz	Beamwidth arcmin	FD Jy	References
102.0	48×25	77.0 ±11.0	1994, Kovalenko et al.
408.0	3.4×3.8	15.0±1.5*	this paper
1420.0	9×9	8.0±0.8	1981, Reich & Braunfurth
1420.0	1×1.12	10.6±0.6*	this paper
2695	4.3×4.3	6.3±1.1	see text
2700.0	4.6×4.6	4.7 ±0.4	1981, Reich & Braunfurth

Mavromatakis et al. (2005) imaged G116.5+1.1 in narrow band optical filters and obtained optical spectra of several bright filaments inside and northeast of the radio SNR. These yield line ratios indicative of shock heated gas which extends about 20 arcmin to the northeast of G116.5+1.1. We have studied the HI maps from the CGPS which have the clearest association with the outline of the radio SNR in the range -41 to -45 km s $^{-1}$. That HI map (their fig. 4), interestingly, has a gap in HI just where the shocked optical filaments extend beyond the boundary of the radio SNR. This suggests that the optical filaments are a breakout region from G116.5+1.1 but not a separate SNR. From the HI velocity Mavromatakis et al. (2005) proposed that G116.5+1.1 is in the Perseus arm. However, this contradicts the conclusion in Yar-Uyaniker

et al. (2004) that it is a local arm SNR, based on detection of polarized radio emission. Neither argument is conclusive but the distance from Yar-Uyaniker et al. is probably better, due to the confusion limited nature of the HI emission in the galactic plane.

4.3 G116.9+0.2 (CTB 1)

Published integrated flux densities for CTB 1 are given in Table 5, and shown in Figure 4 (right). For CTB 1 the correction for compact source flux density is less important than for the other two SNRs, though the correction is important for the spectral indices derived from the subregions C and D (Fig. 1). The best fit spectral index to all seven data points is 0.65, with $\chi^2=8$. The 102 MHz point is above the power-law fit, and the 5 GHz point is below it. Fitting without the 102 MHz and 5 GHz points gives a power-law which agrees with all of the remaining data points, with $\alpha=0.51$ ($\chi^2=2.8$) and 90% range 0.37 to 0.64. This fit is shown in Figure 4 (right). Next we carry out a fit including the 102 MHz and 5 GHz points, but use a synchrotron aging model. This gives $\alpha = 0.56$ ($\chi^2 = 4.8$), a 90% range 0.29 to 0.63, and a turnover frequency of 2.9 GHz.

Table 5 Integrated Flux Densities (FD) of G116.9+0.2

Freq. MHz	Beamwidth arcmin	FD Jy	References
102.0	48 × 25	51.0±10.0	1994, Kovalenko et al.
408.0	3.4×3.8	15.0±1.5*	this paper
610.0	16×20	10.9±1.0	1971,1973, Willis & Dickel
1400.0	9.7×9.7	9.4±1.5	1971,1973, Willis & Dickel
1420.0	9×9	7.8±0.8(7.1)	1981, Reich & Braunfurth
1420.0	2×2	8.3±0.5(7.6)	1982, Landecker et al.
1420.0	1×1.13	8.1±0.4*	this paper
1667.0	22×22	5.5±2.0	1973, Willis, A.G.
2695	4.3×4.3	6.1±1.0	see text
2700.0	4.6×4.6	4.8±0.4(4.45)	1981, Reich & Braunfurth
2740.0	5×5	4.2±0.4 (3.85)	1974, Velusamy & Kundu
5000.0	6.8×6.8	3.0±0.3 (2.8)	1977, Angerhofer et al.

The value in ‘()’ means compact sources’ contributions have been subtracted from the SNR’s flux density by using 610 and 1410 MHz fluxes and the spectral index of its compact sources (Dickel & Willis 1980). *The flux density excludes compact sources.

The different methods for determining the spectral index of CTB 1 all agree and yield a value consistent with the best determined value of 0.48 ± 0.01 from the $T-T$ plot method. The spectral fit to multi-frequency flux density values gives weak evidence (1.6σ) for a spectrum turnover by 0.5 in spectral index at a frequency around 2.9 GHz. A more accurate measurement of the 5 GHz flux density could confirm this result. Here we show that a turnover at $\nu_b=2.9$ GHz is quite feasible for CTB 1. From ν_b , we obtain the electron break energy $E_b = 1.9 \times 10^{-9} (B/2\mu\text{G})^{-0.5}$ J, with B the magnetic field in the synchrotron emitting plasma. An initial power law distribution of electrons will, over time, have a break in its energy spectrum by 1.0 in the energy index at E_b , with E_b increasing with time, t , according to (e.g. Longair 1981): $E_b = (a_s B^2 t)^{-1}$, a_s being the synchrotron energy loss coefficient for energy loss by a single electron: $dE/dt = -a_s B^2 E^2$. The restriction that the turnover frequency ν_b gives is a relation between the age of the supernova remnant and its magnetic field. For $\nu_b=2.9$ GHz, $t = 2.7 \times 10^8 (B/2\mu\text{G})^{-3/2}$ yr. So if CTB 1 is 10^4 yr old, the magnetic field will be 1.8 mG. Evidence for high magnetic field and high density for CTB 1 is given by the optical observations of Fesen et al. (1997), particularly for the bright emission along the western limb.

Finally we note evidence for spectral index variations in CTB 1 (see Fig. 1 and Table 1). Regions A, B, D, E and F are consistent with a spectral index of 0.50. The southern limb (region C) is flatter ($\simeq 3\sigma$). This could be caused by variations in the shock causing electron spectrum variations or by variations in the magnetic field hence in the synchrotron aging. However, to confirm these results and to study the matter further, higher spatial resolution observations are required at 408 MHz.

5 CONCLUSIONS

New observations of G114.3+0.3, G116.5+1.1, and G116.9+0.2 (CTB 1) at 408 MHz have been combined with their 1420 MHz observations in a study of the spectral index of these three SNRs. We remove the effect of compact sources' flux densities in the calculation of the spectral indices by the method of $T-T$ plot and integrated flux densities. We also use published integrated flux densities and correct these for compact sources. The resulting spectral indices for the three SNRs are consistent: 0.37 for G114.3+0.3, 0.38 for G116.5+1.1, and 0.51 for CTB 1. The first two have larger uncertainties due to the faintness of the SNRs and background variations. For CTB 1, the spectral index is very well determined, perhaps the best yet of any supernova remnant. There is some evidence for a spectral turnover in the radio spectrum of CTB 1 near 3 GHz, which can be interpreted as due to synchrotron aging in a strong (mG) magnetic field, consistent with the optical observations of Fesen (1997).

Acknowledgements We acknowledge supports from the Natural Sciences and Engineering Research Council of Canada. The DRAO is operated as a national facility by the National Research Council of Canada. The Canadian Galactic Plane Survey is a Canadian project with international partners.

References

- Angerhofer P. E., Kundu M. R., Becker R. H., 1977, *A&A*, 55, 11
Dickel J. R., Willis A. G., 1980, *A&A*, 85, 55
Fesen R. A., Winkler P. F., Rathore Y. et al. , 1997, *AJ*, 113, 767
Fürst E., Reich W., Reich P., Reif K., 1990, *A&AS*, 85, 691
Haslam C. G. T., Salter C. J., Stoffel H., Wilson W. W., 1982, *A&AS*, 47, 1
Kovalenko A. V., Pynzar A. V., Udalt'sov V. A., 1994, *AR*, 38, 95
Landecker T. L., Roger R. S., Dewdney P. E., 1982, *AJ*, 87, 1379
Leahy D. A., Roger R. S., 1998, *ApJ*, 505, 784
Leahy D. A., Tian W. W., 2005, *A&A*, 440, 929
Lockman F. J., 1989, *ApJS*, 71, 469
Longair M., 1981, *High Energy Astrophysics*, Cambridge: Cambridge University Press
Mavromatakis F., Boumis P., Xilouris E. et al. , 2005, *A&A*, 435, 141
Reich W., Braunsfurth E., 1981, *A&A*, 99, 17
Reich W., Reich P., Fürst E., 1990, *A&AS*, 83, 539
Reich W., Reich P., Fürst E., 1997, *A&AS*, 126, 413
Taylor A. R., Gibson S. J., Peracaula M., 2003, *AJ*, 125, 3145
Tian W. W., Leahy D. A., 2005, *A&A*, 436, 187
Tian W. W., Leahy D. A., 2006, *A&A*, 447, 205
Velusamy T., Kundu M. R., 1974, *A&A*, 32, 375
Willis A. G., 1973, *A&A*, 26, 237
Willis A. G., Dickel J. R., 1971, *ApJ*, 8, L203
Yar-Uyaniker A., Uyaniker B., Kothes R., 2004, *ApJ*, 616, 247